Bioactive Materials 8 (2022) 505–514

Contents lists available at ScienceDirect

Bioactive Materials

journal homepage: www.sciencedirect.com/journal/bioactive-materials

Cryo-self-assembled silk fibroin sponge as a biodegradable platform for enzyme-responsive delivery of exosomes

Muyang Sun [a,b,1], Qi Li [a,1], Huilei Yu [a,1], Jin Cheng [a], Nier Wu [b], Weili Shi [a], Fengyuan Zhao [a], Zhenxing Shao [a], Qingyang Meng [a], Haifeng Chen [b,***], Xiaoqing Hu [a,**], Yingfang Ao [a,*]

[a] Department of Sports Medicine, Institute of Sports Medicine of Peking University, Beijing Key Laboratory of Sports Injuries, Peking University Third Hospital, 49 North Garden Road, Haidian District, Beijing, 100191, China

[b] Department of Biomedical Engineering, College of Future Technology, Peking University, Beijing, 100871, China

ARTICLE INFO

Keywords:
Exosomes
Silk fibroin
Cryo-sponge
Sustained drug delivery
Enzyme-responsive

ABSTRACT

Although advances in protein assembly preparation have provided a new platform for drug delivery during tissue engineering, achieving long-term controlled exosome delivery remains a significant challenge. Diffusion-dominated exosome release using protein hydrogels results in burst release of exosomes. Here, a fibroin-based cryo-sponge was developed to provide controlled exosome release. Fibroin chains can self-assemble into silk I structures under ice-cold conditions when annealed above the glass transition temperature. Exosome release is enzyme-responsive, with rates primarily determined by enzymatic degradation of the scaffolds. *In vivo* experiments have demonstrated that exosomes remain in undigested sponge material for two months, superior to their retention in fibrin glue, a commonly used biomaterial in clinical practice. Fibroin cryo-sponges were implanted subcutaneously in nude mice. The exosome-containing sponge group exhibited better neovascularization and tissue ingrowth effects, demonstrating the efficacy of this exosome-encapsulating strategy by realizing sustained release and maintaining exosome bioactivity. These silk fibroin cryo-sponges containing exosomes provide a new platform for future studies of exosome therapy.

1. Introduction

In recent decades, advances in utilizing peptide and protein self-assembly for the design of novel biomaterials and therapeutics have attracted much attention from researchers in the drug delivery field [1]. Besides the advantages of protein biocompatibility and multiple available sites for adding a wide variety of functional groups [2], self-assembly of natural protein motifs (α-helices, β-sheets, β-hairpins, etc.) supports the assemblies' responsiveness to external cues, including temperature, pH, and enzyme activity, which can be taken advantage of to facilitate controlled drug [3]. A classical peptide-assembly strategy for drug delivery is to incorporate a drug into a self-assembling monomer, then instigate conditions that facilitate peptide self-assembly into polymeric structures [4]. Although this method can achieve precisely regulated delivery of functional therapies on a molecular scale, it cannot deliver drugs with complex compositions, including exosomes.

Exosomes represent a subtype of extracellular vesicles. They are formed by endosomes, and are released by various cell types, to play roles in intercellular communication via autocrine, paracrine, and telocrine pathways [5]. As a new bioactive nanomedicine strategy, the use of exosomes is superior to cell therapy in terms of immunogenicity and safety [6]. Because exosomes are enveloped by a lipid bilayer with a size distribution ranging from 40 to 160 nm [7], self-assembly between peptides conjugated to exosome membranes is largely sterically restrained. A general delivery strategy based on peptide self-assembly involves passive encapsulation of exosomes into peptide hydrogels [8,9]. However, after being soaked in PBS solution, the hydrogels release quantities of exosomes by diffusion at an initial release rate during the first few days that is faster than the rehabilitation rate of damaged tissues, including cartilage and meniscus [10,11]. Although adding clays

Peer review under responsibility of KeAi Communications Co., Ltd.

* Corresponding author.
** Corresponding author.
*** Corresponding author.
E-mail addresses: haifeng.chen@pku.edu.cn (H. Chen), huxiaoqingbd01@sina.com (X. Hu), aoyingfang@163.com (Y. Ao).

[1] These authors contributed equally to this work.

https://doi.org/10.1016/j.bioactmat.2021.06.017
Received 2 January 2021; Received in revised form 11 June 2021; Accepted 11 June 2021
Available online 22 June 2021

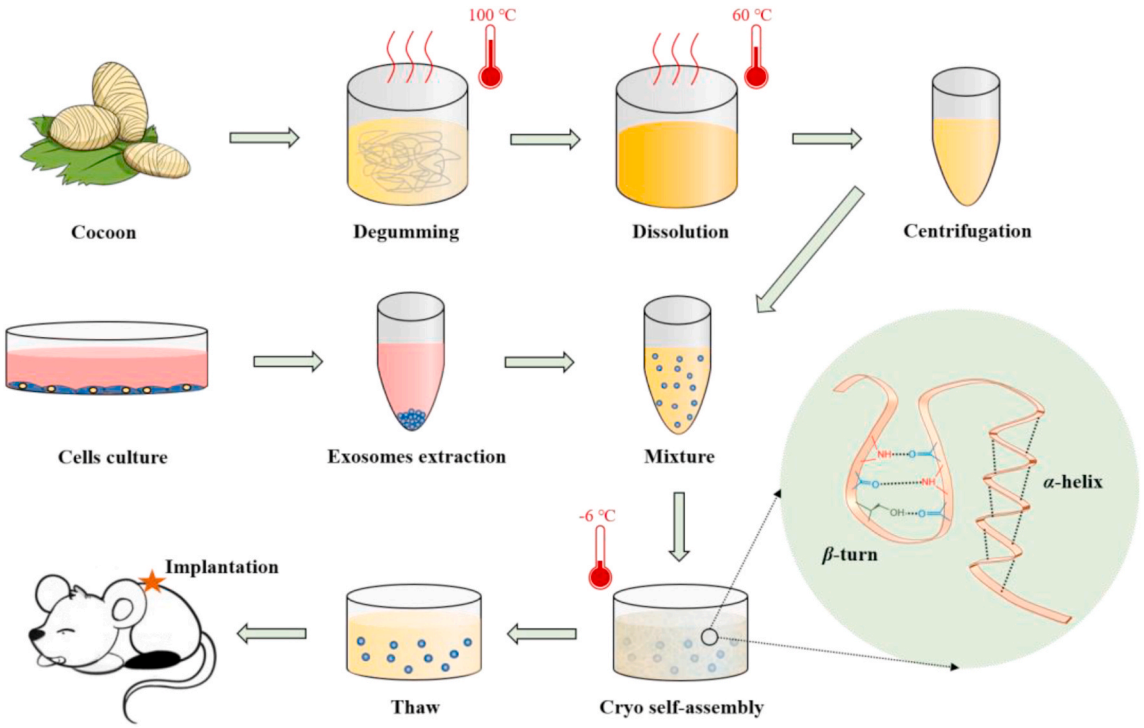

Fig. 1. Scheme illustrating the overall study.

such as laponite into hydrogels can retard exosome release, and has shown a promising effect on periodontal tissue reconstruction [12], the inorganic component may lead to calcification when implanted into soft tissues [13]. Therefore, it is essential to develop novel preparation strategies for peptide assemblies that can achieve sustained exosome release.

Silk fibroin (SF) is a natural amphipathic protein extracted from *Bombyx mori* silk that has been widely studied as a drug delivery candidate because of its excellent biodegradability [14]. As a result of the repetitive presence of Gly-X (X being Ala, Ser, Thr, Val) motifs within hydrophobic blocks, many protocols have been proposed to induce SF self-assembly [15]. However, since high SF concentrations are prone to spontaneous self-assembly and precipitation, the guided protein assembly process can only be conducted at low concentrations (usually less than 20%, empirically) and under mild conditions. The product is mainly a hydrogel, and its drug release profile is largely diffusion rate limited [16]. Compared with other methods, the ice cold phase-separation technique offers promise for overcoming this problem [17]. When a macromer solution is frozen and annealed below 0 °C, the polymeric molecular chains will separate from the solvent ice and crosslink under conditions that allow higher concentrations to be used [18]. As the reaction temperature is close to the glass transition temperature of the macromer, the motion of the molecular chains is restrained, slowing self-assembly and allowing increased macromer concentrations. We thus explored a novel method for fabricating fibroin-based cryo-sponges for sustained exosome release.

In the present study, a novel platform was established that can achieve long-term steady release of bone marrow mesenchymal stem cell (BMSC) derived exosomes together with scaffold degradation (Fig. 1). SF cryo-sponge preparation was controlled by freezing, followed by annealing above the glass transition temperature (T_g) of the SF solution. The mechanism of SF cryo-self-assembly below 0 °C was investigated using combined data collected by FTIR, XRD, SEM, and differential scanning calorimetry (DSC). Exosomes entrapped in fibroin sponge network maintained their membrane integrity, resulting in an obviously degradation-limited release profile compared with the fibrin glue group, as demonstrated by *in vitro* experiments and subcutaneous implantation in nude mice. To verify whether this exosome-encapsulating strategy could deliver sustained release of functional exosomes, SF sponges loaded with or without exosomes were implanted subcutaneously in nude mice. Biocompatibility of the SF cryo-sponges, and nascent tissue ingrowth into the sponges were examined to assess the effects of sustained exosome release on internal scaffold regeneration.

2. Materials and methods

2.1. Fibroin protein extraction

Fibroin purification was performed using a method described by Rockwood [19]. *Bombyx mori* cocoon (15 g) was cut into pieces and boiled for 30 min in 0.02 mol/L Na_2CO_3 to remove sericin proteins. Silk fibroin was then rinsed three times with water and dried overnight. Extracted silk was dissolved in a 9.3 M/L LiBr solution (the weight ratio between silk and LiBr was 1:4) for 4 h at 60 °C. This fibroin solution was dialyzed against DI water for 3 days. The mixture was then centrifuged twice at 9000 rpm for 20 min at 4 °C. Supernatants were frozen in liquid nitrogen and lyophilized for storage.

2.2. SF cryo-sponge and traditional sponge preparation

To dissolve, lyophilized SF sponge was carefully placed into a centrifuge tube without squeezing. After adding PBS, the centrifuge tube was shaken up and down violently for 1 min to mix well, then centrifuged at 4000 rpm for 5 min to remove any non-soluble SF. SF concentration was determined by weighing the mass of the solution after drying. Supernatants were frozen at −80 °C for 30 min, annealed at −5 °C for 2 days, then thawed (CSF). To prepare traditional sponge (ESF), SF solution was lyophilized, then immersed in ethanol for 2 h, and washed with PBS.

2.3. Preparation and characterization of BMSC exosomes

Rat BMSCs were isolated according to a previously reported protocol

[20]. Briefly, bone marrow was isolated from femurs and tibia of Sprague-Dawley rats weighing 80 g. Cells isolated from the bone marrow were incubated in α-minimal essential medium (α-MEM). After culturing for 4–5 days, adherent cells reached confluence and were defined as passage 0. Passage 3 cells were used in all experiments. Exosomes were prepared and characterized following a previously described protocol [21]. Briefly, cells were cultured for 48 h, then the conditioned medium (CM) was collected for exosome isolation by differential centrifugation at 4 °C. Exosomes were resuspended in PBS and preserved at −80 °C. Average particle size among the purified exosomes was measured by nanoparticle tracking analysis (NTA) measurements using Nanosight (Malvern). Exosome morphology was verified by transmission electron microscopy (TEM, JEM1400PLUS).

2.4. Fabrication of exosome-encapsulating SF cryo-sponges

To fabricate exosome-containing SF cryo-sponges (SF-exos), 50 μL of exosomes (3×10^6/μL) was mixed with 100 μL of 15% SF (dissolved in 0.75 × PBS) yielding a mixture with a final concentration of 10% SF and 1×10^6/μL exosomes (ionic strength equal to 0.5 × PBS). The mixture was frozen at −80 °C for 30 min and annealed at −5 °C for 2 days. To fabricate exosome-containing fibrin glue for a control group (Fibrin-exos), 40 μL of exosomes (3×10^6/μL) was mixed with 20 μL of thrombin (500 IU/mL) and 60 μL of fibrinogen (50 mg/mL).

2.5. Differential scanning calorimetry (DSC)

DSC measurements were conducted using a Q 100 differential scanning calorimeter (TA, USA). The SF solution was poured into a sealed aluminum cell swept with N_2 gas during analysis. Scanning rate, heating rate, and sample weight were 10 °C/min, 10 °C/min, and 7.26 mg, respectively.

2.6. Fourier transform infrared spectroscopy (FTIR)

SF sponges were crushed into powder form and assayed by Affinity-1S FTIR spectrometry (SHIMADZU, Japan). The detected range was 4000–400 cm^{-1}. Resolution and scanning frequency were 4 cm^{-1} and 5 times, respectively. A second derivative analysis was performed on the spectra to identify all hidden peaks. Fourier self-deconvolution of the spectra for the amide I region (1700-1600 cm^{-1}) was performed using peaks analysis in Origin 9.0 (OriginLab Corporation, USA). Deconvolution was performed using the Lorentzian peak type, and the reduced chi-square for curve fitting was controlled under 1×10^{-4}. Secondary structure contents were calculated by summing the areas of the relative peaks.

2.7. X-ray diffraction analysis (XRD)

The crystalline regions of the lyophilized sponges were examined by XRD with Cu Kα radiation (λ = 1.5405) at 40 kV and 100 mA.

2.8. Scanning electron microscopy (SEM)

Scaffold morphologies were observed by scanning electron microscopy (SEM; JSM-7900F, JEOL, Japan) with an accelerating voltage of 3 kV. Samples were frozen at 80 °C for 12 h, then lyophilized. Lyophilized samples were gold-coated using a Gatan Model 691PIPS (Gatan, USA) before observation.

2.9. Mechanical characterization of the sponge

Compressive and tensile strength tests were performed using an AGS-X Precision Universal Tester (SHIMADZU, Japan) with a 50 N load cell. Five samples were prepared from each group. For the compressive test, sponges were prepared in a cylindrical mold with a diameter of 15.6 mm, and a height of nearly 10 mm. For tensile tests, samples were cut into cuboids (40 × 10 mm) with a thickness of 1–2 mm. Crosshead speeds were set constant at 0.5 mm/min and 3 mm/min for compressive and tensile tests, respectively. (n = 5).

2.10. Enzymatic degradation profile of sponges

Proteinase K solution was used for *in vitro* enzymatic degradation experiments. Enzyme solutions were diluted in 1 × PBS to 0.4 U/mL for final testing concentration. After weighing a lyophilized sponge sample (~5 × 5 mm, 3 mm height), the sample was immersed in enzyme solution (2 mL, 37 °C). Enzyme solution was changed every 2 days. On days 0, 1, 2, 4, 6, and 8, the remaining sponge sample was removed, washed in PBS, lyophilized, and weighed. The results are shown as the residual mass fraction of the initial dry weight (n = 5).

2.11. Fluorescent labeling of exosomes

For quantification of exosomes released from SF cryo-sponges *in vitro*, PKH 67 (Sigma, USA) was used to label exosomes. A suspension containing 2×10^9 exosomes (30 μL) was prepared in an Eppendorf tube, 4 μL PKH ethanolic dye solution to 1 mL of Diluent C in another Eppendorf tube, and then mixed. The exosome/dye suspension was incubated for 5 min, then staining was stopped by adding 1% BSA. Samples were incubated for 1 min to allow binding of excess dye. The solution was then centrifuged at 100,000×*g* for 70 min. The sediment, containing exosomes labeled with PKH67, was re-suspended in PBS, and preserved at −80 °C.

For quantification of exosomes released from SF cryo-sponges *in vivo*, DiR was used to label exosomes. A suspension containing 2×10^9 exosomes (30 μL) was prepared in an Eppendorf tube and incubated in a solution containing 5 μM DiR dye. The exosome/dye suspension was incubated for 5 min, then centrifuged at 100,000×*g* for 70 min. The sediment, containing DiR-labeled exosomes was re-suspended in PBS, then preserved at −80 °C.

2.12. Assessment of the structural integrity of exosomes released from scaffolds

SF-exosome scaffolds were cut into pieces and digested with proteinase K solution (0.1 U/mL) at 37 °C. To minimize enzymatic damage to exosome membranes, the enzyme solution was centrifuged every hour at 4000 rpm for 3 min. Supernatants were collected and mixed with equal volumes of 1% BSA to stop digestion. Precipitants were resuspended in fresh enzyme solution. Exosomes were collected and extracted from supernatants using the same protocol used to extract exosomes from cells. TEM and nanoparticle tracking analysis (NTA) were used to characterize exosome morphology and size distribution.

2.13. Analysis of the exosome release-degradation profile from SF cryo-sponges in vitro

To quantify exome release from scaffolds *in vitro*, exosomes were labeled with PKH 67. A concentration gradient of labeled exosomes was used to establish an exosome concentration standard curve using a twofold serial dilution method. The standard curve maximum concentration was 1×10^7 exosomes/μL. SF-exosome sponges and fibrin-exosome gels containing 1×10^6 exosomes/μL were prepared for the following experiment. Sponges were cut into 5 mm × 5 mm × 0.3 mm fragments. Proteinase K solution (0.4 U/mL) was used for enzymatic exosome release and scaffold degradation experiments, while PBS was used for the hydrolytic experiment. Scaffolds were immersed in 0.5 mL of degradation solution. On days 1, 2, 3, 4, 5, 6, 8, and 10, 0.2 mL of supernatant was collected and neutralized with 0.2 mL of 1% BSA solution. Fresh degradation solution was then added. After 10 days, the remaining scaffolds were digested with 4 U/mL of proteinase K solution

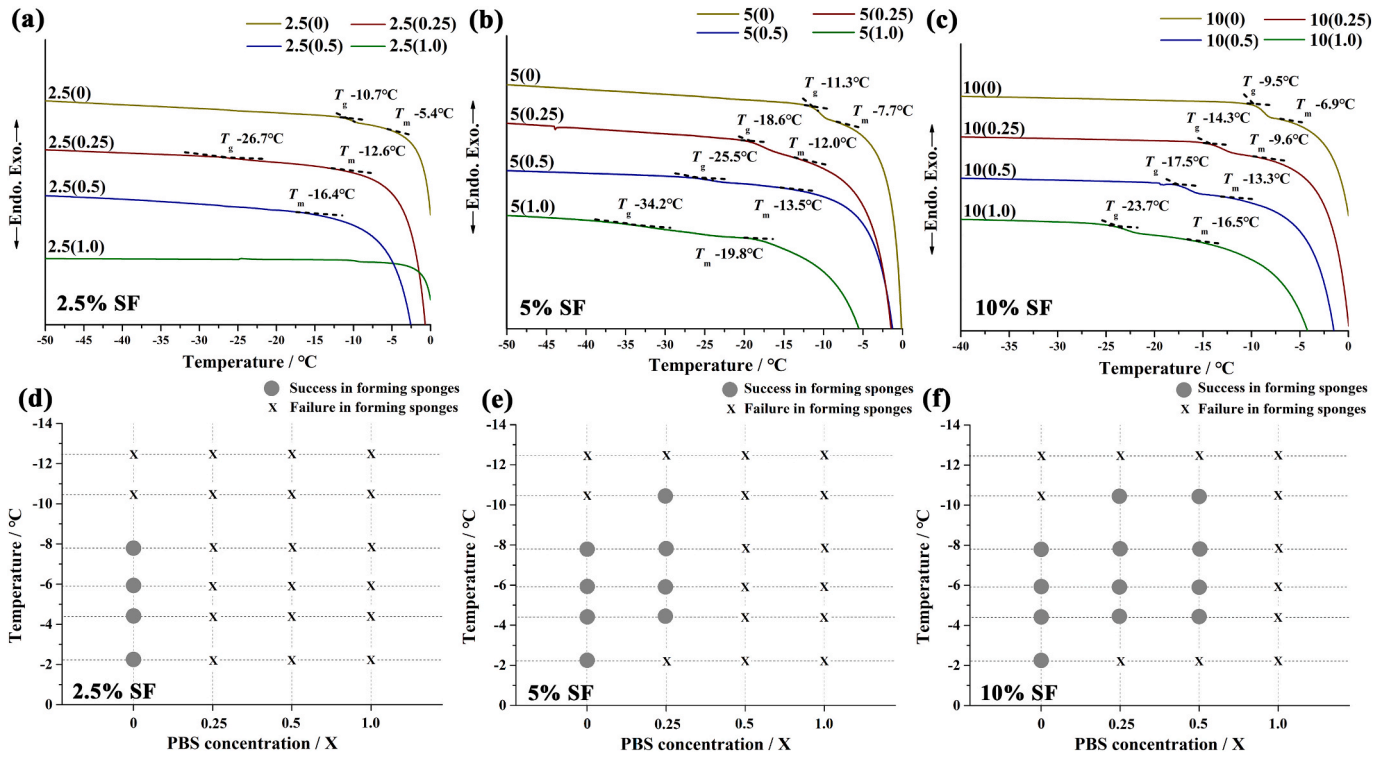

Fig. 2. Measurement of T_g for SF solutions, and recording of successful preparation of SF cryo-sponges under different conditions. a-c) DSC rewarming curves for 2.5% (a), 5% (b) and 10% (c) SF solutions with 4 different ionic strengths (SF dissolved in 0 x, 0.25 x, 0.5 x, and 1.0 x PBS). d-f) Recording of the results of SF cryo-sponge preparation using 2.5% (d), 5% (e) and 10% (f) SF solutions with different annealing temperatures and ionic strengths. T_g: glass transition temperature of an SF solution; T_m: melting temperature of an SF solution.

and neutralized. The number of released labeled exosomes per day was detected using a varioscan flash (excitation wavelength: 485 nm; emission wavelength: 600 nm) and calculated based on the standard curve. The cumulative degree of exosome release is shown as the ratio of released exosomes per day to total exosomes encapsulated in the scaffold. To measure the degree of scaffold degradation in the enzymatic/hydrolytic environment, 5 mm × 5 mm × 0.3 mm cubes of scaffold were lyophilized and weighed, then immersed into a 0.5 mL degradation solution. On days 1, 2, 3, 4, 5, 6, 8, and 10, the remaining scaffold was removed, washed 3 × with PBS lyophilized, and weighed. The results are shown as the residual mass fraction relative to initial dry weight (n = 4).

2.14. Animal studies

All animal experimental protocols were approved by the local Institutional Animal Care and Use Committee (Peking University Biomedical Ethics Committee), in compliance with the "Guide for the Care and Use of Laboratory Animals" published by the National Academy Press (NIH Publication No. 85–23, revised 1996). Exosomes were labeled in advance of use with DiR. For evaluation of exosome release *in vivo*, 32 nude mice (6–8 weeks old) were randomly divided into two groups, then incised (5 mm) in the skin on their backs. Each group was implanted with SF-exosome or Fibrin-exosome, separately. At weeks 1, 3, 5, and 8, four mice per group were selected for live fluorescent imaging and immunofluorescence assessment. Eight nude mice (6–8 weeks old) in which scaffolds without exosomes were seeded (control) were harvested after 1 week. For *in vivo* exosome function evaluation, 12 nude mice (6–8 weeks old) were incised (5 mm) in the skin on their backs, and randomly divided into two groups. These groups were seeded with SF-exosomes, or SF cryo-sponges without exosomes. At weeks 4 and 8, three mice per group were harvested for H&E staining and immunohistochemical assessment.

2.15. Living fluorescent analysis and immunofluorescence assessment

An IVIS Spectrum Imaging System (Xenogen, USA) was used to detect fluorescent signals in mice with labeled exosomes, and semi-quantitatively analyze the data. At certain time point, nude mice were anesthetized and placed in the machine under air anesthesia conditions (excitation wavelength: 745 nm). After fluorescent imaging, the mice were sacrificed, and the remaining SF-exosome sponges were collected for immunofluorescence assessment. Detailed protocols for immunofluorescence assessment are provided in Supporting Information.

2.16. Histological assessment

Residual subcutaneously seeded SF-exosomes and SF sponges were collected and fixed in paraformaldehyde for 48 h, dehydrated in a gradient of alcohol soaks, and embedded in paraffin blocks. Histologic sections (5 μm) were prepared using a microtome and stained with hematoxylin and eosin (H&E), or immunohistochemically stained for VEGFR and α-SMA. Detailed protocols for H&E staining are provided in Supporting Information.

2.17. Statistical analysis

Data are presented as means ± standard deviation. Data analysis was performed using Origin 9.0. Unpaired t-tests were used for two group comparisons. Statistical significance was set at $p < 0.05$.

3. Results and discussion

3.1. Measurement of T_g of the SF solution

Formation of cryogels and cryo-sponges is driven by enhanced crosslinking between highly concentrated macromers, which are

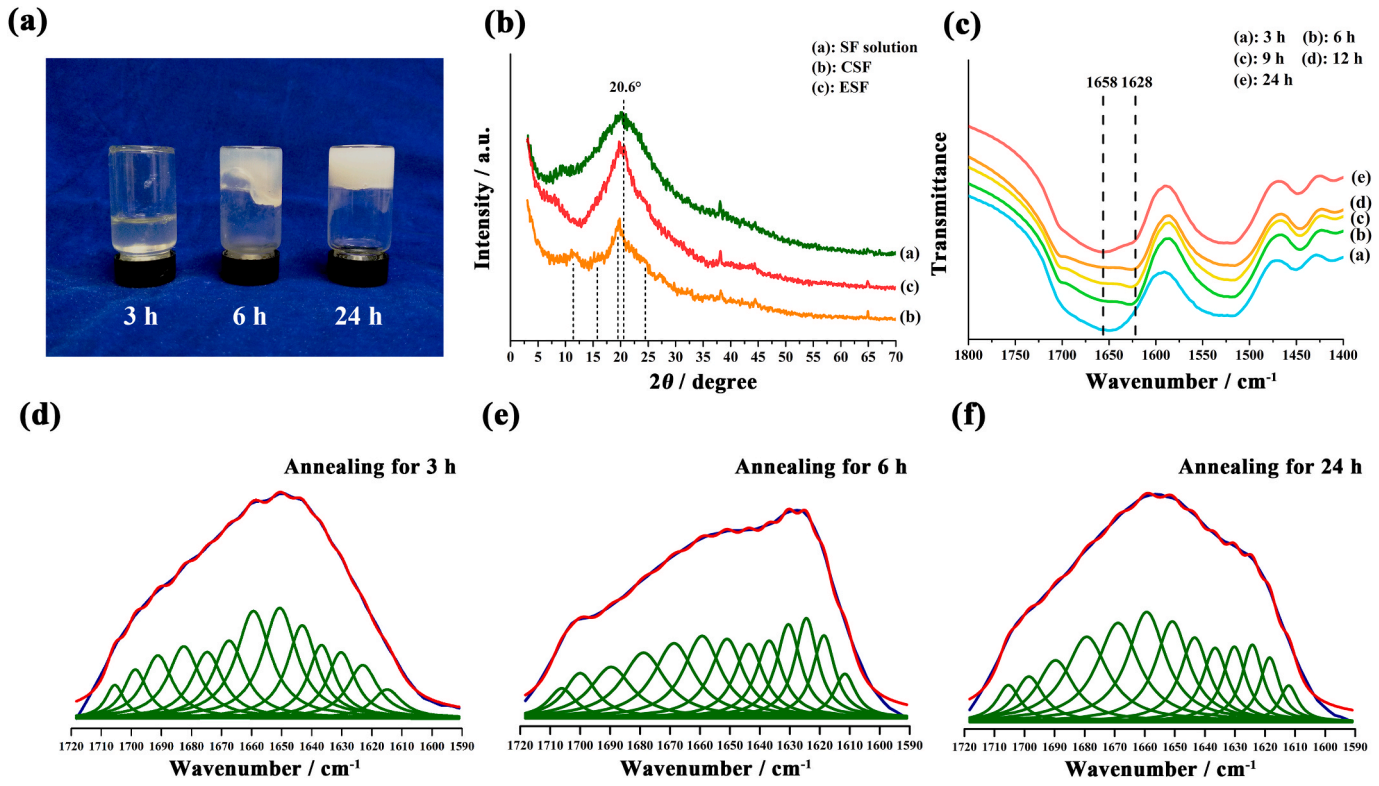

Fig. 3. Analysis of fibroin cryo-sponge structure. a) 5% SF solution annealed at around −6 °C for 3 h, 6 h and 24 h. b) X-ray diffraction patterns of SF solution, CSF, and ESF. c) FTIR spectra of fibroin solution annealed at around −6 °C for 3, 6, 9, 12 and 24 h. d-f) Deconvoluted FTIR curves of SF solution annealed at around −6 °C for 3, 6 and 24 h. Blue, red, and green curves represent the original FTIR spectrum, the spectral fit, and 13 deconvoluted curves.

expelled from freezing solvent crystals and entangled within limited regions. High concentration solutes reduce solvent vapor pressure relative to pure solvent, resulting in the coexistence of ice crystals and concentrated polymer solutions when the annealing temperature is between T_g and the melting point of the solvent. It is thus essential to determine the T_g of the solution for preparing cryo-sponges. The T_g of the polymer solution was obtained during heating from −80 °C to 0 °C, from each solution's DSC curve (Fig. 2a–c). For the SF solutions prepared by dissolving the protein in DI water (2.5(0), 5(0), 10(0)), the onsets of T_g were all approximately −10 °C. T_g was also measured for SF solutions with different molecular weights. No differences in T_g values were observed (Figure S1).

For carbohydrate solutions, glass transition temperature and solvent melting point have been widely investigated based on DSC rewarming scans [22], including the silk fibroin solution studied by Li et al. [23]. However, these results (−34 °C to −20 °C) are quite different from our measurements. Given that solutions containing SF of different molecular weights have the same T_g (Figure S1), we hypothesize that different dissolution reagents (Libr and $CaCl_2$–EtOH–H_2O) may lead to different glass transition behaviors.

Because exosomes are extracellular vesicles, osmotic pressure is important for maintaining the integrity of their membrane structures. We thus investigated the effect of solution ionic strength on T_g. To our knowledge this question has not been previously addressed. Increasing ionic strength significantly shifted T_g to lower temperatures. Increasing SF concentration suppressed this trend. When SF was dissolved in 0.5 x PBS, T_g for a 2.5% SF solution could not be determined, but a 10% SF solution retained a T_g of −23.7 °C. These results demonstrate that SF self-assembly in an ice-cold state is significantly influenced by ion content. This phenomenon may be caused by a salting-out effect (Na^+ salts) [24]. During this process, the number of water molecules bound to peptide chains decreases, resulting in a more tightly entangled conformation of peptide chains in the frozen state, and a lower T_g for the fibroin solution.

3.2. Temperature-dependence of time required for formation of SF cryo-sponges

To further elucidate the effects of SF concentration, ionic strength, and annealing temperature on the process of SF self-assembly, SF solutions were frozen and annealed at temperatures between 0 °C and −24 °C for three days. Samples were taken every 12 h and thawed. The time required for the SF solution to transform into cryo-sponges was also recorded (Fig. 2d–f, Table S1). A DIY low-temperature annealing box was designed to avoid interference from temperature fluctuations caused by the refrigerator (Figure S2). For SF solutions with zero ionic strength, all three groups (2.5(0), 5(0), and 10(0)) could self-assemble into sponges, and displayed a trend toward temperature dependence when annealed between −7.8 °C and −2.2 °C. Self-assembly speed increased with increasing annealing temperature, and was inhibited by addition of PBS.

3.3. Analysis of the structural transition of fibroin during cryo-treatment

FTIR spectra were used to assess the secondary structure of SF cryo-sponges (CSF). These results were compared with those of a traditional SF sponge prepared by ethanol treatment (ESF) (Figure S3). The SF solution exhibited its main peaks at 1650 cm^{-1} and 1534 cm^{-1}, indicating that the majority of SF in solution formed random coils. The CSF spectrum's main peaks were at 1658 cm^{-1} and 1526 cm^{-1}, supporting a structural transformation from random coils to α-helix [25]. A shoulder peak at 1628 cm^{-1} indicated the existence of β-sheet. For comparison, an obvious peak shift to lower wavenumbers was observed in the spectrum of ESF, with strong peaks at 1628 cm^{-1} and 1518 cm^{-1}, demonstrating an increase in antiparallel β-sheet structure [26].

Structural changes in SF sponges were also assessed by XRD (Fig. 3b).

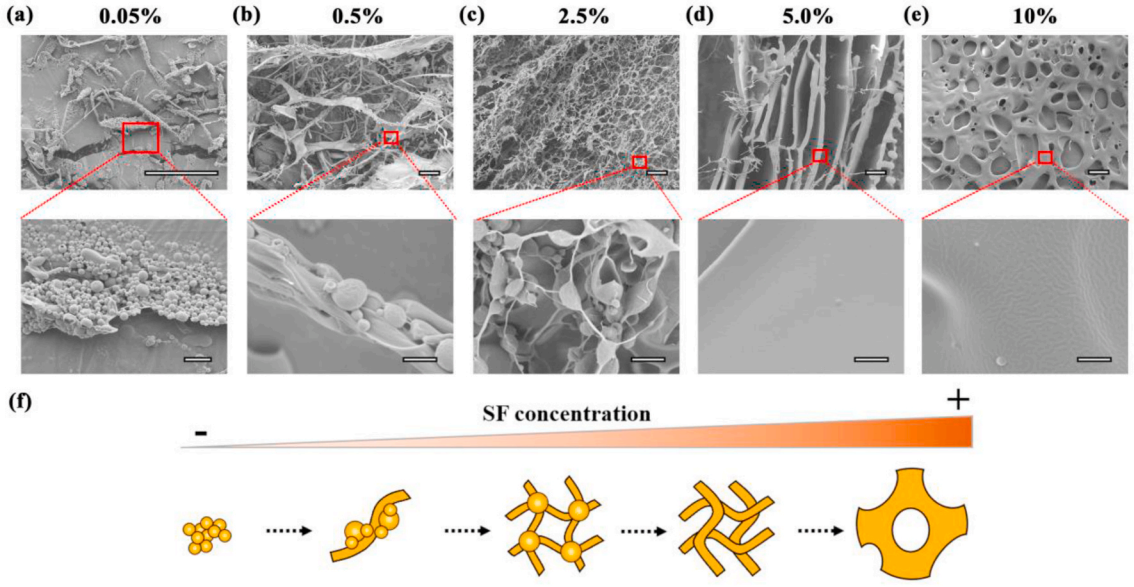

Fig. 4. SEM images of cryo-sponges with different fibroin concentrations: a) CSF-0.05, b) CSF-0.5, c) CSF-2.5, d) CSF-5, e) CSF-10. f) Scheme depicting fibroin protein self-assembly from nanoscale to microscale. Scale bar: a-e) 20 μm; enlarged images of a-e) 2 μm.

The SF solution presented a broad peak at approximately 20°, indicating an amorphous structure. The ESF sponges showed a distinct peak at 20.6°, with two shoulder peaks at 8.7° and 24°, indicating the presence of *β*-crystalline structure (silk II) [27]. The peak at 19.8° was a characteristic peak of silk I structure, indicating a mixture of silk I and silk II in ESF. CSF showed peaks at 11.9°, 15.7°, 19.8°, and 24.5°, corresponding to typical silk I spacing distances of 0.74, 0.56, 0.45, and 0.36 nm [28].

To identify structural changes in SF solution over time during cryo-treatment, a 5% SF solution was annealed at approximately −6 °C for 3, 6, 9, 12, and 24 h. All samples were then stored at 25 °C (RT) for 24 h to observe whether the following phase transition occurred. Samples were then lyophilized. The SF solution showed no change during annealing for 3 h. After 6 h of annealing, the SF solution transformed into a soft hydrogel immediately after thawing (Fig. 3a) and became tough after storage at RT. The main peak of the spectrum shifted to 1628 cm^{-1} (Fig. 3c). As treatment time increased, the intensity of the peak at 1628 cm^{-1} decreased, while that at 1658 cm^{-1} intensified. After annealing for 24 h, the SF solution self-assembled into a sponge, and the main peak of the spectrum shifted to 1658 cm^{-1}.

Fourier self-deconvolution and curve-fitting were carried out to further explore the change in secondary structure during cryo-treatment (Fig. 3d–f, Figure S4). These vibration bonds were assigned by referring to the literature [29]. With annealing time extension, more SF proteins were transformed into *α*-helical structures with β-turns. As conformations containing β-sheet are more stable than other secondary structures, transition from β-sheets to *α-helices* and β-turns is almost impossible. The decline in β-sheet content may result from formation of crystalline silk I structure. During the annealing process, fibroin chains (especially secondary structures such as turns and helices) generally self-assemble to form silk I structure. After thawing, a lower ratio of free turns and

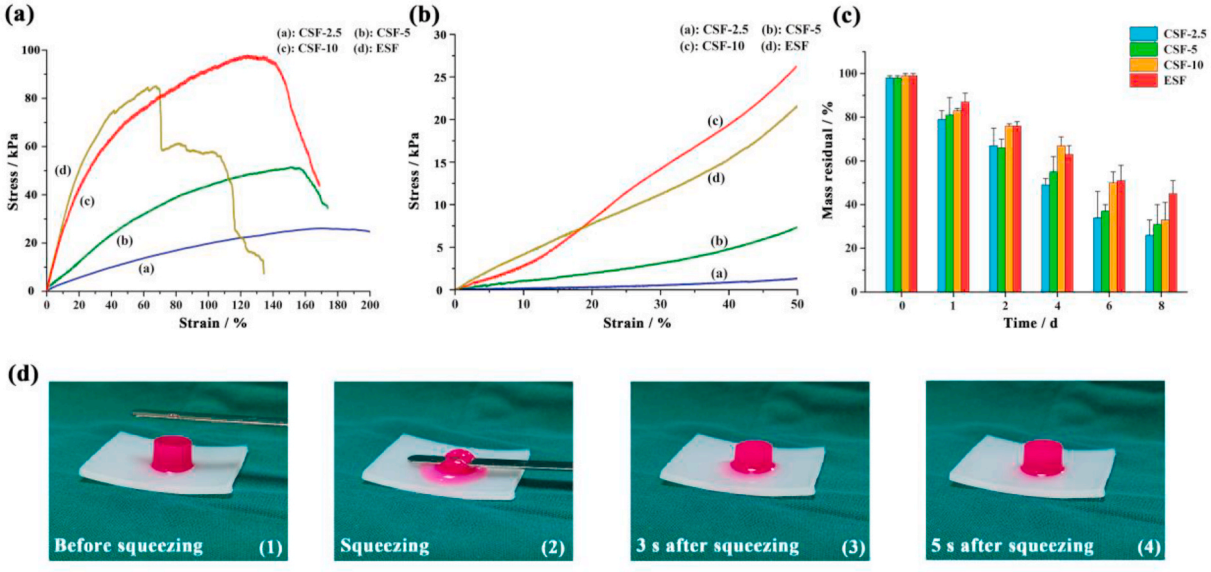

Fig. 5. Mechanical properties and degradation profiles of CSF compared with ESF. CSF sponges were prepared with different SF concentrations (2.5%, 5%, and 10%), while ESF sponges were prepared using 5% SF. a) Tension stress-strain curves. b) Compressive stress-strain curves. c) Enzymatic degradation of fibroin sponges. d) SF cryo-sponges displayed good ductility and fast water absorption (within 5 s) after being fully squeezed. ($n = 3$).

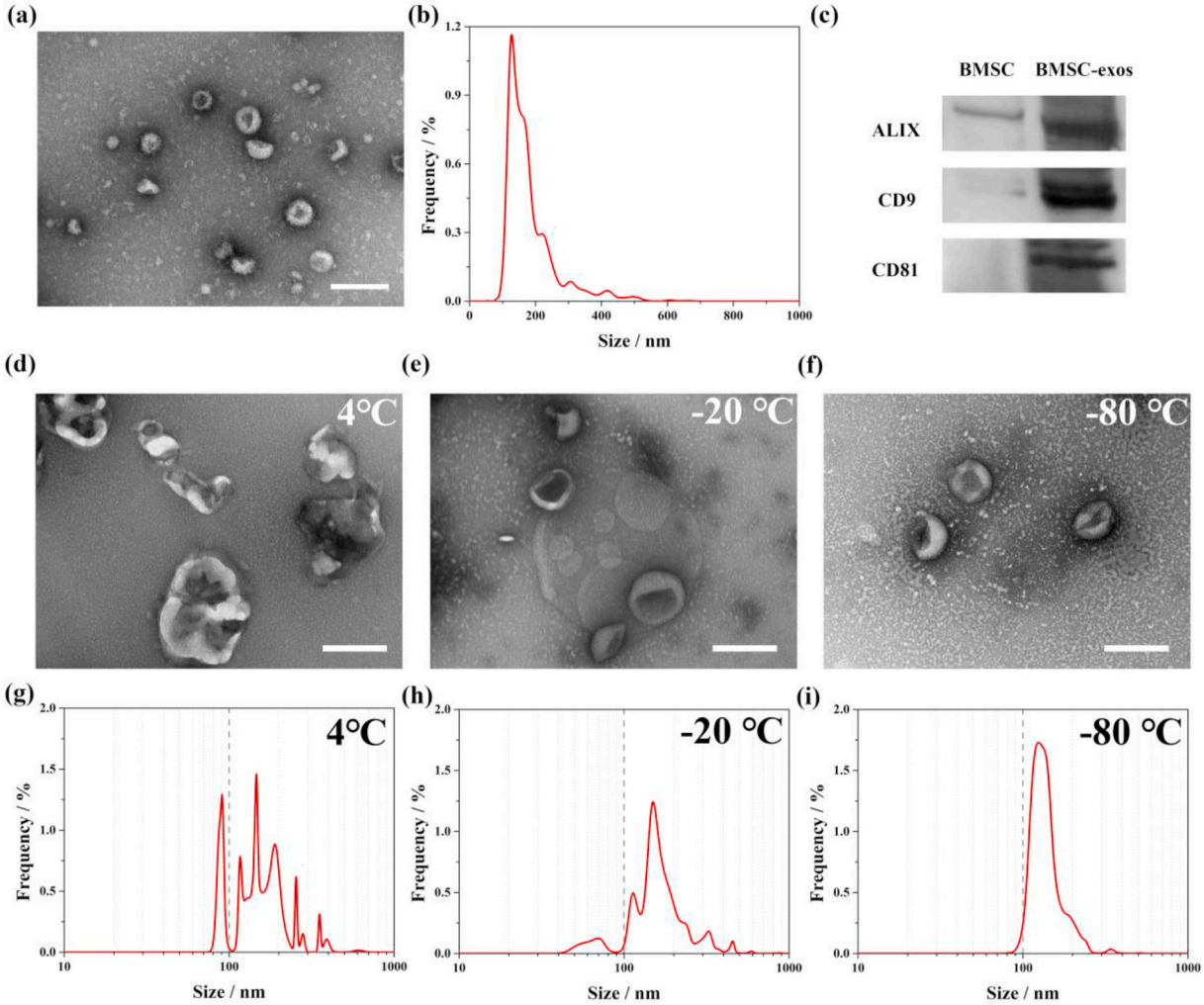

Fig. 6. SF cryo-sponges maintained exosome structural integrity during long-term storage. a-c) Identification of BMSC-derived exosomes by TEM, nanoparticle tracking analysis (NTA), and western blotting for ALIX, CD9, and CD81. d-f) Morphological changes in sponge-encapsulated exosomes after storage for 1 mouth at 4, −20, and −80 °C. g-h) Size distribution of sponge-encapsulated exosomes after 1 month's storage at 4, −20, and −80 °C. Scale bar: 200 nm. ($n = 3$).

helices existed with increasing annealing time, which translates to self-assembly of β-sheets when SF hydrogels were stored at RT. After 24 h of annealing, all chains self-assembled into a silk I structure. No further phase transition could be observed when the SF cryo-sponges were stored at RT.

Morphological characteristics of SF cryo-sponges were observed using SEM to analyze the relationship between SF concentration and final product morphology (Fig. 4a–e). Samples were quickly frozen at −80 °C to reduce any effect of freezing speed on morphology, after which, samples were annealed at −6 °C for two days. The sample containing low concentration (0.05%) SF self-assembled into nanospheres. With increasing SF concentration, the nanospheres became densely arranged, with increasing tendency to fuse into irregular micro bulks with smooth surfaces. At 5% SF, the SF solution self-assembled into a sponge with a smooth hole wall, and nano morphology disappeared.

Experimental data [30,31] show that achieving a silk I structure requires slow concentration of an SF solution at low temperatures, providing sufficient time for the fibroin chains to self-assemble. This transition process may be affected by many factors, such as molecular mobility, hydrophilic/hydrophobic interactions, charge, temperature, and SF concentration, placing significant limits on silk I structural dynamics research. The special biphasic states of SF solutions at their glass transition temperature, however, provide good reaction conditions to produce the silk I structure. Combining the present data with previous studies, we propose a hypothesis to explain this phenomenon.

In the fibroin solution, more than 50% of polymer chains contain irregular secondary structures, including random coils and turns. These turns function as nucleation sites for protein folding [32]. When fibroin molecules are hydrated, the hydrating H_2O molecules are considered to be unable to contribute to ice formation [33]. During solute crystallization, the unfrozen phase concentrates, forming nano-spherical micelles to decrease the interfacial free energy. By contrast to SF micelle formation in solution, during which the hydrophobic domains are encapsulated inside the micelles [34], the hydrophilic domains and their hydrating water molecules would aggregate as solvent ice forms. Therefore, the hydrophobic effect on the proteins is inhibited, and the fibroin self-assembles into a silk I structure. When annealing takes place above T_g, the independent SF micelles can fuse together, forming wires and plates, and eventually forming porous scaffolds with increasing SF concentration (Fig. 4f).

3.4. Mechanical characterization and degradation profile of SF cryo-sponges

SF concentration exerts an important effect on mechanical strength, as shown in the tensile and compressive curves of the CSF sponges (Fig. 5a and b, Table S2). The tensile and compressive moduli of 10% CSF were 250 kPa and 37 kPa, respectively, several times higher than

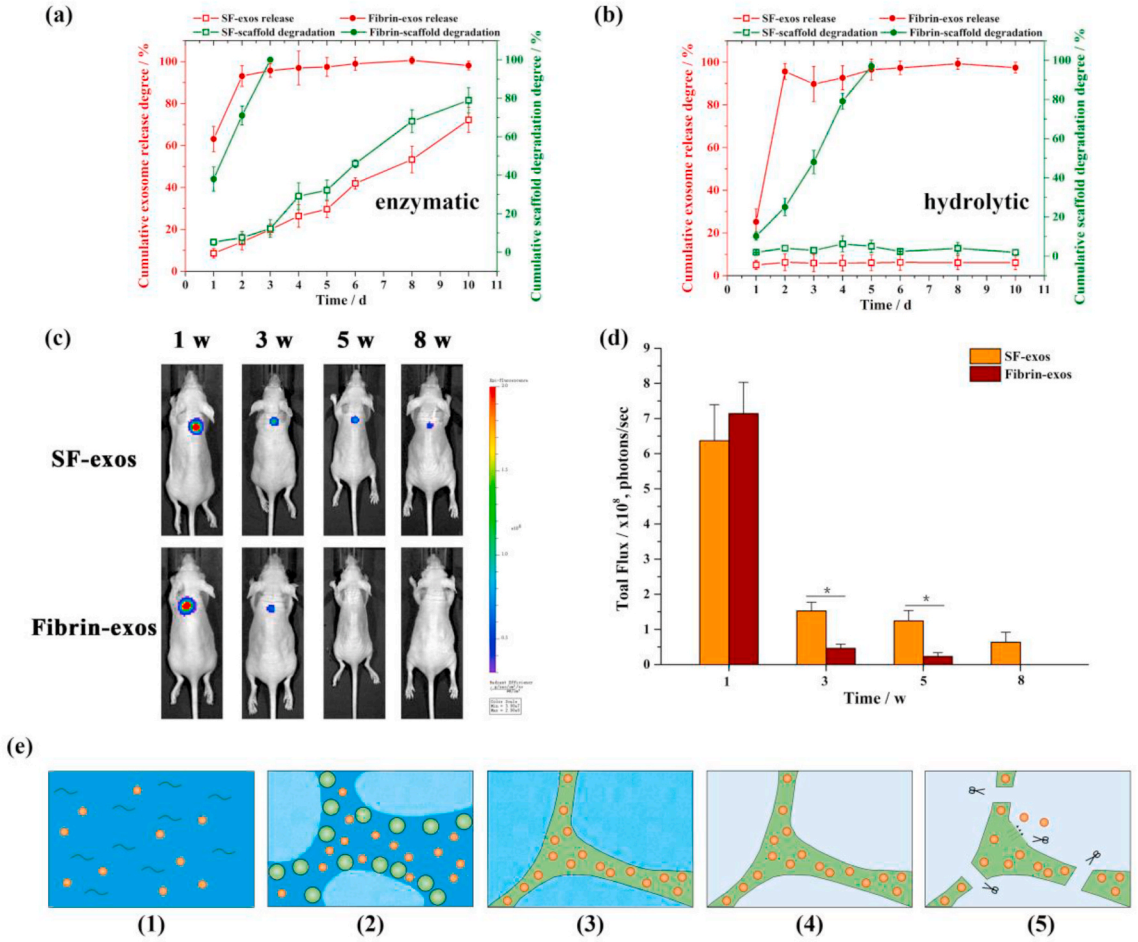

Fig. 7. *Ex vitro* and *in vivo* studies of sustained exosome release from SF cryo-sponges. a) Exosome release and scaffold degradation profiles under enzymatic conditions. b) Exosome release and scaffold degradation profiles under non-enzymatic hydrolytic conditions. c) *In vivo* distribution of scaffold-carried exosomes within 8 weeks. A radiant efficiency scale is presented to the right of mice image. d) Quantitative analysis of total flux at the implantation site using IVIS imaging. e) Schemes depicting mechanisms by preparation strategy for degradation-dominated sustained exosome release via cryo-sponges. ($n = 4$; $^*p < 0.05$).

those of 5% CSF. Compared with ESF (5% SF), CSF also exhibited better ductility. The elastic deformation of CSF-5 was 40%, whereas that of ESF was only 15%. The elongation at breaking point of all CSF groups reached 120%, more than twice that of ESF.

Porous silk fibroin sponges were exposed to an enzyme-containing solution to assess their biodegradation rates (Fig. 5c). The degradation rate of CSF sponges was dependent on fibroin concentration. Sponges with higher fibroin concentrations presented slower degradation rates. Degradation of ESF (5% SF) was slower than that of CSF-5. After 8 days in proteinase solution, 41% of ESF remained, whereas only 21% of CSF-5 remained. A hydrolytic experiment was also carried out using PBS; however, neither CSF nor ESF experienced any mass loss within 21 days (data not shown).

Formation of silk II (ESF) was driven by the hydrophobic effect, where crystalline fibroin β-sheets were entrapped in hydrophobic cores, presenting better thermal stability (Figure S5). By contrast, silk I structures resulted from cryo-self-assembly. The lower percentage of β-sheet resulted in reduced mechanical strength, while increased turn and helix content led to better ductility and water absorption (Fig. 5d). This hydrated structure also easily exposed peptide chains to proteinase compared with silk II, and hence was degraded faster than ESF.

3.5. Maintenance of exosomes' structural integrity in long-term storage

The structural integrity of exosomes in long-term storage was analyzed based on morphological changes and particle size distribution. Based on the results presented above (Fig. 2, Table S1), when 0.5 x PBS was chosen as the solvent, only SF with a concentration of 10% (10(0.5)) could form a sponge. None of the SF solutions could self-assemble into CSF when dissolved in 1.0 × PBS. Therefore, 10% SF (dissolved in 0.5 × PBS) was selected as the experimental condition for subsequent exosome-related experiments. TEM images showed that fresh BMSC exosomes were hemispherical, with particle diameters of approximately 127 nm (Fig. 6a–c), consistent with previously described exosomes [21,35]. After encapsulating exosomes in CSF, sponges were stored at 4, −20, or −80 °C for one month, separately. When stored at −80 °C, exosomes released from the CSF retained their original shape, with a diameter distribution of around 124.5 nm (Fig. 6f, i). Exosome aggregation and fusion occurred at −20 °C, although exosome structural integrity was maintained (Fig. 6e,h). By contrast, all exosomes broke into angular shapes at 4 °C (Fig. 6d,g). At low osmotic pressures, damage to exosome membranes at 4 °C may result from excessive swelling of liposomes.

In a previous study, exosome storage at low temperatures (lower than 0 °C) without addition of cryoprotectants was shown to change exosome morphology [36]. Lipid bilayers may be damaged by ice crystals during freezing, and exosomes may fuse during dehydration. In our study, exosome morphology remained stable when stored at −80 °C for a month, in accordance with NTA results. We speculate that during the freezing process, exosomes become isolated by fibroin chains, inhibiting exosome fusion. When stored at 4 °C, exosomes exhibited swelling and membrane disruption. This phenomenon resulted from

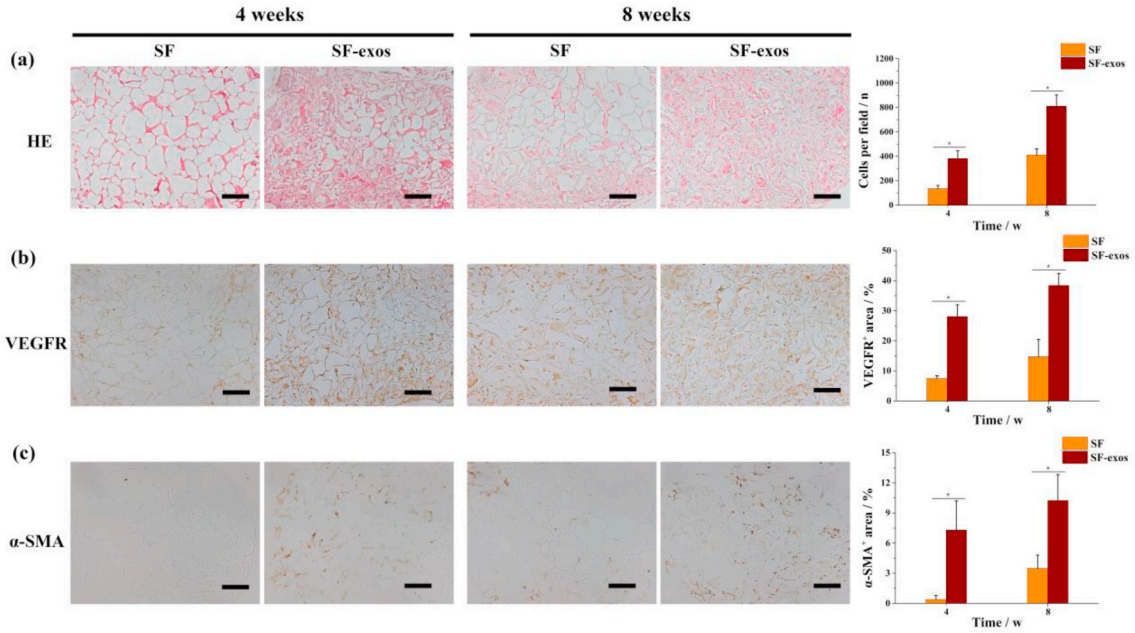

Fig. 8. Histological evaluation after 8 weeks' implantation, of exosome function upon release from SF-sponge-exosomes. SF sponges without exosomes were implanted into a control group. a) Representative H&E stained images of scaffolds, and quantitative analysis of cellular ingrowth per imaging field over 8 weeks. b) Immunohistochemistry images of VEGFR, and statistical analysis of data. c) Immunohistochemistry images of α-SMA, and statistical analysis of data. Scale bar: 100 μm. ($n = 3$; $^*p < 0.05$).

storage in a solution with low osmotic pressure.

3.6. Degradation-dominated exosome release behavior of CSF sponges

To analyze the mode of exosome release from SF cryo-sponges, we first compared the release profiles of scaffolds with their degradation rates in enzymatic and non-enzymatic hydrolytic environments. Fibrin glue, which has been widely used in clinical surgeries and has been proven to reduce the release rate of exosomes for better tissue regeneration outcomes, was used as a control group [21]. Under enzymatic hydrolytic conditions, both fibrin glue and SF scaffolds exhibited continuous degradation, and exosome release occurred together with scaffold digestion (Fig. 7a). In the non-enzymatic hydrolytic environment, however, the exosomes in SF sponges (SF-exosome) were hardly released (Fig. 7b). On the first day, less than 5% of exosomes leaked, which may be due to insufficient fibroin self-assembly. Exosomes in fibrin glue (Fibrin-exos) exhibited a burst release in the first 2 days, which was faster than the fibrin scaffold degradation rate.

Sustained exosome release was also verified *in vivo* using a nude mouse subcutaneous implantation model. Exosomes were labeled with DiR for exosome tracking and fluorescent quantification *in vivo* (Fig. 7c and d). The fibrin exosome group showed a significant decrease in fluorescence intensity by week 3, and no fluorescent signal could be detected in week 8. By contrast, the DiR fluorescent label of the SF-exosome groups remained visible after two months. As we have demonstrated that the time required for complete release of exosomes from fibrin glue is less than one week, the fluorescent signal detected in the fibrin glue group after one week should be attributed to DiR detachment from endocytosed exosomes. Therefore, immunofluorescence staining was performed to locate fluorescing cells and residual exosomes in the SF-exosome group (**Figure S6**). After 8 weeks, DiR-labeled exosomes can still be observed in area free of proliferated cells, which represents undegraded SF sponges. The above results indicate that loading exosomes in SF cryo-sponges achieved long-term sustained release of exosomes, regulated by scaffold degradation.

Based on our experimental data on the formation of SF cryo-sponges, we propose the following explanation for degradation-rate limited exosome release (Fig. 7e). During the freezing of SF-exosome solution, unfrozen fibroin chains are transformed from random coil structure into nanospheres, which then fuse into a smooth block with few hydrating water molecules trapped inside. During this phase separation process, exosomes gradually aggregate within the hydrophilic core of the peptide structures. By the end of phase separation, SF has self-assembled into scaffolds with a silk I structure while encapsulating exosomes inside the cryo-sponge structure they form. When SF-exosome sponges are immersed in PBS, the folded peptide displays resistance to non-enzymatic hydrolytic degradation, preventing exosome release through water diffusion. However, when exposed to enzymatic hydrolysis, the proteinase can disrupt the peptide network, releasing exosomes, and thereby achieving degradation-rate limited exosome release.

3.7. The in vivo function of exosomes released from SF-sponge-exosomes

To verify the functional efficacy of this exosome release strategy, SF-exosome cryo-sponges were implanted subcutaneously on the backs of nude mice to examine cellular ingrowth and neovascularization. SF sponges without embedded exosomes were incapable of recruiting cells into the sponge, as demonstrated by H&E staining at week 4 (Fig. 8a). Neovascularization and myofibroblast ingrowth were almost undetectable. The SF-exosome groups stimulated remarkable neo-angiogenesis and cellular ingrowth (Fig. 8b). Quantitative analysis of non-vascular α-SMA-positive pixels (myofibroblast tissue) indicated that the response of myofibroblasts was greater than that in response to control sponges at weeks 4 and 8 (Fig. 8c). The role of MSC-derived exosomes in angiogenesis has been extensively studied. Exosomes transfer several growth factors and miRNAs to endothelial cells, promoting the transcription of many molecules involved in angiogenesis. In this study, exosomes were gradually released as the SF sponges were degraded, stimulating vessel formation and cell migration, while active metabolic processes also accelerated scaffold degradation. The dynamic balance between scaffold degradation and tissue ingrowth prevented formation of empty cavities inside the scaffolds, a feature that may provide benefits for better tissue rehabilitation.

4. Conclusion

In summary, a novel silk fibroin scaffold produced by cryo-self-assembly was developed for degradation rate limited exosome release. Fibroin chain self-assembly was achieved by phase separation under ice-cold conditions at a temperature above the glass transition temperature of the fibroin solution, which led to formation of the rare silk I structure. This structure yields fibroin sponges with higher ductility and a faster degradation rate than those of the traditional silk II structure. During phase separation, exosomes were gradually tightly encapsulated by fibroin chains, making exosome release solely dependent on enzymatic scaffold degradation. Sustained exosome release promoted cell migration and formation of new blood vessels, as well as ingrowth of myofibroblasts. Degradation-dominated sustained exosome release, based on fibroin cryo-sponges, may offer a new direction for exosome-related applications to long-term tissue rehabilitation and regeneration. Because of these cryo-sponges' efficacy in long-term preservation of exosomes at low temperatures, it is also of great significance for clinical application of exosomes to tissue engineering.

Declaration of competing interest

The authors declare no conflicts of interest.

CRediT authorship contribution statement

Muyang Sun: Conceptualization, Data curation, Investigation, Methodology, Project administration, Writing – original draft. **Qi Li:** Conceptualization, Data curation, Investigation, Methodology, Project administration, Writing – original draft, and. **Huilei Yu:** Conceptualization, Data curation, Investigation, Methodology, Project administration, Writing – original draft. **Jin Cheng:** Writing – review & editing, Conceptualization, Formal analysis. **Nier Wu:** Data curation, Methodology. **Weili Shi:** Funding acquisition, Investigation, Project administration, Resources. **Fengyuan Zhao:** Funding acquisition, Investigation, Project administration, Resources. **Zhenxing Shao:** Funding acquisition, Investigation, Project administration, Resources. **Qingyang Meng:** Funding acquisition, Investigation, Project administration, Resources. **Haifeng Chen:** Writing – review & editing, Conceptualization, Formal analysis. **Xiaoqing Hu:** Writing – review & editing, Conceptualization, Formal analysis. **Yingfang Ao:** Conceptualization, Project administration, Writing – review & editing, Funding acquisition.

Acknowledgements

M.S., Q.L., and H. Y. contributed equally to this work The authors gratefully acknowledge support from the Natural Science Foundation of Beijing Municipality (No. 7171014), National Natural Science Foundation of China (No. 81871770, 81802101, 81802153), National Key Research and Development Program of China (No. 2016YFC1101301, 2018YFF0301100), and Beijing Nova Program Z201100006820011.

Appendix A. Supplementary data

Supplementary data to this article can be found online at https://doi.org/10.1016/j.bioactmat.2021.06.017.

References

[1] G.B. Qi, Y.J. Gao, L. Wang, H. Wang, Adv. Mater. 30 (22) (2018), e1703444, https://doi.org/10.1002/adma.201703444, 1703444-n/a.
[2] P. Katyal, F. Mahmoudinobar, J.K. Montclare, Curr. Opin. Struct. Biol. 63 (2020) 97–105, https://doi.org/10.1016/j.sbi.2020.04.007.
[3] N. Habibi, N. Kamaly, A. Memic, H. Shafiee, Nano Today 11 (1) (2016) 41–60, https://doi.org/10.1016/j.nantod.2016.02.004.
[4] C.J.C. Edwards-Gayle, I.W. Hamley, Org. Biomol. Chem. 15 (28) (2017) 5867–5876, https://doi.org/10.1039/C7OB01092C.
[5] D.M. Pegtel, S.J. Gould, Annu. Rev. Biochem. 88 (1) (2019) 487–514, https://doi.org/10.1146/annurev-biochem-013118-111902.
[6] B. Yang, Y. Chen, J. Shi, Adv. Mater. 31 (2) (2019), e1802896, https://doi.org/10.1002/adma.201802896, 1802896-n/a.
[7] Kalluri, R.; LeBleu, V. S., Science 2020, 367 (6478).
[8] C. Han, J. Zhou, B. Liu, C. Liang, X. Pan, Y. Zhang, Y. Zhang, Y. Wang, L. Shao, B. Zhu, J. Wang, Q. Yin, X.Y. Yu, Y. Li, Mater. Sci. Eng. C Mater. Biol. Appl. 99 (2019) 322–332, https://doi.org/10.1016/j.msec.2019.01.122.
[9] C. Han, J. Zhou, C. Liang, B. Liu, X. Pan, Y. Zhang, Y. Wang, B. Yan, W. Xie, F. Liu, X.Y. Yu, Y. Li, Biomater. Sci. 7 (7) (2019) 2920–2933.
[10] W. Shi, M. Sun, X. Hu, B. Ren, J. Cheng, C. Li, X. Duan, X. Fu, J. Zhang, H. Chen, Y. Ao, Adv. Mater. 29 (29) (2017) 28585319, https://doi.org/10.1002/adma.201701089.
[11] Z. Li, N. Wu, J. Cheng, M. Sun, P. Yang, F. Zhao, J. Zhang, X. Duan, X. Fu, J. Zhang, X. Hu, H. Chen, Y. Ao, Theranostics 10 (11) (2020) 5090–5106, https://doi.org/10.7150/thno.44270.
[12] W. Shi, S. Guo, L. Liu, Q. Liu, F. Huo, Y. Ding, W. Tian, ACS Biomater. Sci. Eng. 6 (10) (2020) 5797–5810.
[13] S.T. Koshy, D.K.Y. Zhang, J.M. Grolman, A.G. Stafford, D.J. Mooney, Acta Biomater. 65 (2018) 36–43.
[14] W. Huang, S. Ling, C. Li, F.G. Omenetto, D.L. Kaplan, Chem. Soc. Rev. 47 (17) (2018) 6486–6504, https://doi.org/10.1039/c8cs00187a.
[15] Y. Wang, J. Guo, L. Zhou, C. Ye, F.G. Omenetto, D.L. Kaplan, S. Ling, Adv. Funct. Mater. 28 (52) (2018), https://doi.org/10.1002/adfm.201805305, 1805305-n/a.
[16] J. Li, D.J. Mooney, Nat. Rev. Mater. 1 (12) (2016), https://doi.org/10.1038/natrevmats.2016.71.
[17] O. Okay, Adv. Polym. Sci. 263 (2014) iii–iv, https://doi.org/10.1007/978-3-319-05846-7.
[18] K.R. Hixon, T. Lu, S.A. Sell, Acta Biomater. 62 (2017) 29–41, https://doi.org/10.1016/j.actbio.2017.08.033.
[19] D.N. Rockwood, R.C. Preda, T. Yücel, X. Wang, M.L. Lovett, D.L. Kaplan, Nat. Protoc. 6 (10) (2011) 1612–1631, https://doi.org/10.1038/nprot.2011.379.
[20] Z. Shao, X. Zhang, Y. Pi, X. Wang, Z. Jia, J. Zhu, L. Dai, W. Chen, L. Yin, H. Chen, C. Zhou, Y. Ao, Biomaterials 33 (12) (2012) 3375–3387.
[21] H. Yu, J. Cheng, W. Shi, B. Ren, F. Zhao, Y. Shi, P. Yang, X. Duan, J. Zhang, X. Fu, X. Hu, Y. Ao, Acta Biomater. 106 (2020) 328–341.
[22] Y. Roos, M. Karel, Int. J. Food Sci. Technol. 26 (6) (1991) 553–566.
[23] M. Li, S. Lu, Z. Wu, H. Yan, J. Mo, L. Wang, J. Appl. Polym. Sci. 79 (12) (2001) 2185–2191.
[24] T. Arakawa, S.N. Timasheff, Biochemistry 23 (25) (1984) 5912–5923.
[25] J. Ming, B. Zuo, J. Appl. Polym. Sci. 125 (3) (2012) 2148–2154, https://doi.org/10.1002/app.36354.
[26] W. Xiao, W. Liu, J. Sun, X. Dan, D. Wei, H. Fan, J. Bioact. Compat Polym. 27 (4) (2012) 327–341, https://doi.org/10.1177/0883911512448692.
[27] T. Asakura, A. Kuzuhara, R. Tabeta, H. Saito, Macromolecules 18 (10) (1985) 1841–1845, https://doi.org/10.1021/ma00152a009.
[28] Q. Lu, X. Hu, X. Wang, J.A. Kluge, S. Lu, P. Cebe, D.L. Kaplan, Acta Biomater. 6 (4) (2010) 1380–1387, https://doi.org/10.1016/j.actbio.2009.10.041.
[29] B.D. Lawrence, F. Omenetto, K. Chui, D.L. Kaplan, J. Mater. Sci. 43 (21) (2008) 6967–6985, https://doi.org/10.1007/s10853-008-2961-y.
[30] J. Ming, F. Pan, B. Zuo, Int. J. Biol. Macromol. 75 (2015) 398–401, https://doi.org/10.1016/j.ijbiomac.2015.02.002.
[31] S. Sohn, H.H. Strey, S.P. Gido, Biomacromolecules 5 (3) (2004) 751–757.
[32] A.M. Marcelino, L.M. Gierasch, Biopolymers 89 (5) (2008) 380–391, https://doi.org/10.1002/bip.20960.
[33] T. Uchida, M. Nagayama, T. Shibayama, K. Gohara, J. Cryst. Growth 299 (1) (2007) 125–135.
[34] Q. Lu, H. Zhu, C. Zhang, F. Zhang, B. Zhang, D.L. Kaplan, Biomacromolecules 13 (3) (2012) 826–832.
[35] Q. Li, H. Yu, M. Sun, P. Yang, X. Hu, Y. Ao, J. Cheng, Acta Biomater. 125 (2021) 253–266, https://doi.org/10.1016/j.actbio.2021.02.039.
[36] B. Qin, Q. Zhang, X.M. Hu, T.Y. Mi, H.Y. Yu, S.S. Liu, B. Zhang, M. Tang, J. F. Huang, K. Xiong, J. Cell. Physiol. 235 (11) (2020) 7663–7680.